Read at the Annual Conference of the Ussher Society, January 1995

STRAIN AND SCALING RELATIONSHIPS OF FAULTS AND VEINS AT KILVE, SOMERSET

M. O'N. BOWYER AND P. G. KELLY

Bowyer, M. O'N. and Kelly, P.G. 1995. Strain and scaling relationships of faults and veins at Kilve, Somerset. *Proceedings of the Ussher Society*, **8**, 411-415.

The geometries of well-exposed normal, reverse and strike-slip faults cutting the Lower Lias succession at Kilve, Somerset have been examined. The earliest structures comprise a series of east-west striking normal faults and veins, many showing reverse reactivation. East-west striking reverse faults (reactivated normal), and strike-slip faults conjugate about north-south, are possibly related to this inversion event. Using fault-slip and vein data, the palaeostress orientations for each deformation phase are inferred. North-south extension was followed by north-south contraction, and there has possibly been a period of east-west contraction.

Normal faults, veins and strike-slip faults mapped at scales of 1:20 and 1:1250 each show comparable geometries over several orders of magnitude, and strain measured at different scales shows similar scaling behaviour. The fault displacements obey a power-law scaling relationship, and this is used to estimate the total amount of strain for the structures at all scales of mapping.

M. O'N. Bowyer and P.G. Kelly, Department of Geological Sciences, University of Plymouth, Drake's Circus, Plymouth PL4 8AA.

INTRODUCTION

At Kilve Beach, North Somerset (Figure 1) there are more than three kilometres of exposed Lower Lias limestones and shales in both cliff section and on the wave-cut platform.

Using fault-slip data, the palaeostress orientations have been estimated for the normal, reverse and strike-slip faulting episodes.

Various structures were studied on different scales, to examine how strain has been accommodated. The purpose of studying the different scales was to assess the scaling relationships of both displacement and geometries of faults and veins. Marrett and Allmendinger (1990) state that fault displacements follow power-law distributions, which can be used to quantify the number of faults with a particular displacement. Other examples of phenomena that follow fractal behaviour, such as floods and erosional topography, are discussed by Turcotte (1990).

There are three aims of this study. Firstly, to compare the fault and vein geometries on mapped scales of 1:20 and 1:1250. Secondly, to analyse the brittle strain using extension and contraction values, and power-law scaling relationships, and thirdly to analyse palaeostress orientations using fault-slip data

COMPARISON OF FAULT AND VEIN GEOMETRIES

Brittle structures were mapped at scales of 1:20 and 1:1250 to compare their geometries (Figure 2). The majority of the normal faults and veins are orientated with an approximately east-west strike (Figure 3) and occasionally overstep forming relay-ramps on the fault scale, and bridges on the vein scale (Peacock, 1991). The development of these is described by Peacock and Sanderson (1991). The mean strike orientation of the normal fault is 094-274°, and the

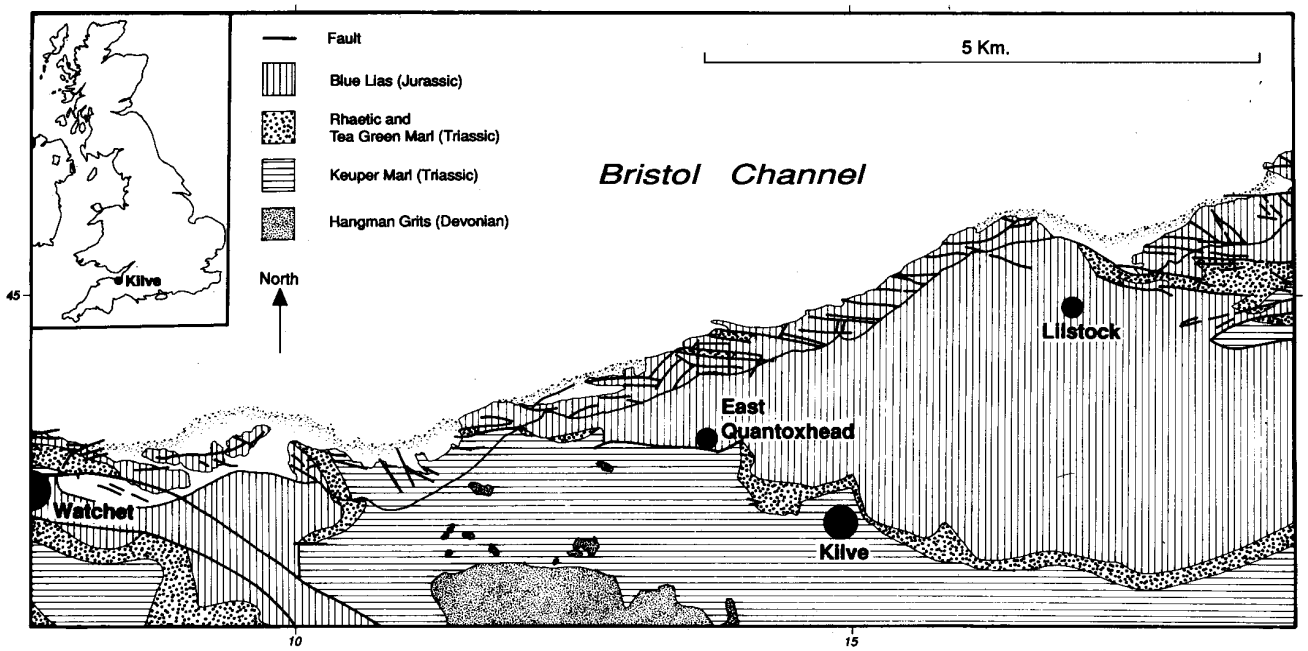

Figure 1. Location map of Kilve Beach, Somerset, U.K (drawn by D.C.P. Peacock after Whitaker and Green, 1979). The square symbol indicates the location of Figure 2 (a).

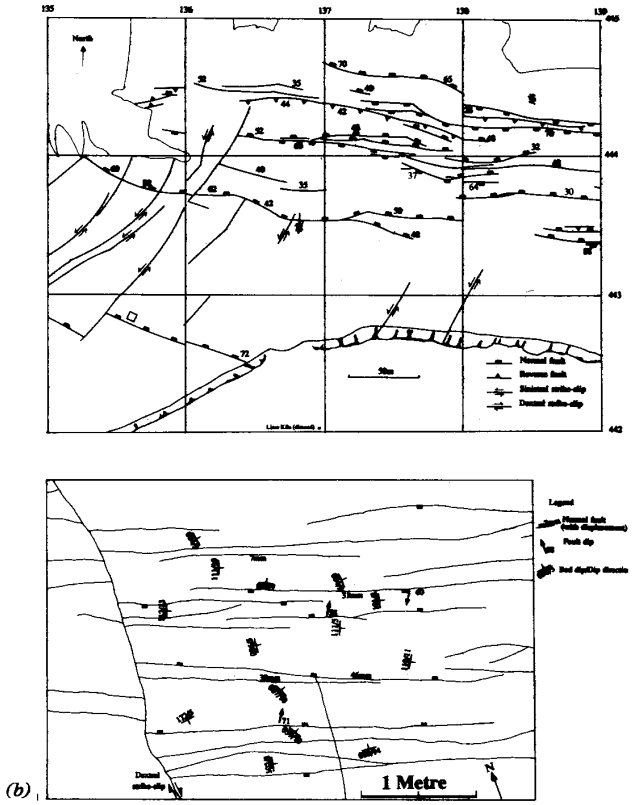

Figure 2. Maps of scale (a) 1:1250 (the square symbol indicates the location of Figure 2 (b)).and (b) 1:20. Note the similarity of the geometries.

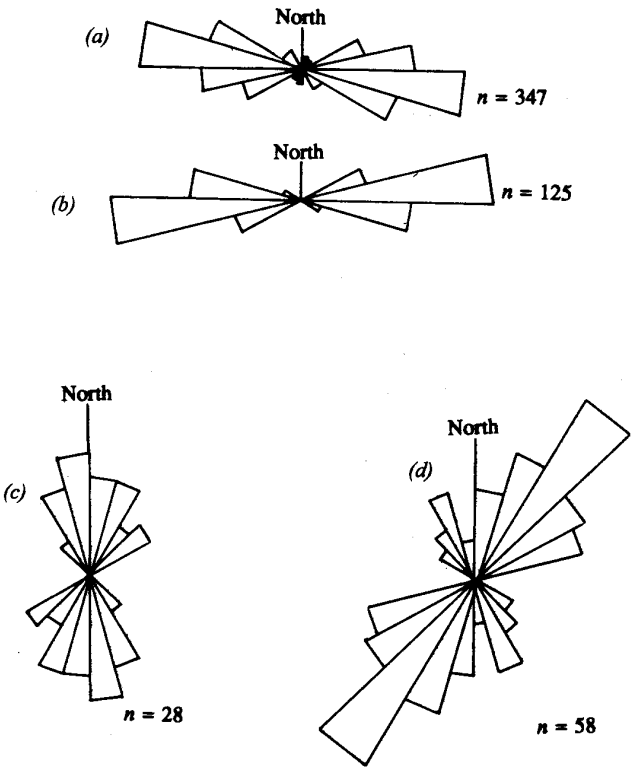

Figure 3. Rose diagrams showing the similarity of the strikes of (a) faults, (b) veins, (c) sinistral strike-slips and (d) dextral strike-slip faults.

veins have a mean strike of 085-265°. Strike-slip faults have orientations of either north-south, north-east—south-west or north-west—south-east (Figure 3). The sense of movement on these fault planes varies, and does not appear to be a function of strike orientation, although dextral displacements dominate the north-west—south-east direction with a modal strike orientation of 172°. The sinistral faults have a modal strike orientation of 38°. The extensional fractures exhibit similar geometries on both mapped scales, suggesting that they formed under similar deformation regimes.

Reverse faults did not appear on the larger mapped scale (1:20), although evidence of reactivation of the normal faults did, including kink banding and deformed veins. On the 1:1250 map, reverse faults show similar east—west orientations to the normal faults, some of which are controlled by reactivation of existing fault planes.

STRAIN ANALYSIS

Strain derived from fault displacements and vein widths.

The majority of the dip-slip faults and veins strike approximately east-west, so fault heave and vein displacement data were collected along a north-south traverse, i.e. normal to the strike. For calculation of the amount of brittle strain from fault heaves, data from 15 line traverses of various lengths between 30 and 120 m were collected. Vein data were collected along two line traverses whose lengths were 1.53 and 11.15 m, independently of fault data (Table 1). Equation 1 can be used to estimate the minimum strain:

$$\%\text{Extension or }\%\text{Contraction} = \frac{(\Sigma h)}{(l - \Sigma h)} \times 100 \quad \text{(Equation 1)}$$

Σh is the sum of the heaves (or the sum of the vein widths), and I is the length of the traverse (after Chapman and Williams, 1984). For the fault displacement data there is 7% average extension, compared to 12% extension for the vein width data. There is also an estimated minimum of 0.2% average contraction (varying from 0.05% to 0.58%) over the measured fifteen fault traverses. The strain estimates are minimum values as they exclude ductile deformation of the wall-rocks, and they do not include faults and veins outside the scale of observation. The analysis of the scaling-relationships of the faults and veins suggests that large, basin-scale faults contribute significantly to the total regional strain. Also, the reactivation event may have reduced the values of the original fault displacements by reversing originally normal faults. The finite displacements are therefore often less than the normal or reverse displacements. The strain derived from vein traverses is indicative of the amount of local extension across a single normal fault zone, as veins were sampled in the wall-rocks. Figure 4 shows examples of cumulative displacement-distance graphs for the normal fault and vein traverses. The gradient is proportional to the displacement per unit distance, and is resolution dependent (Peacock and Sanderson, 1994). The variation of the gradient of the slopes is caused by variations in the amount of displacement of individual fractures, and the fault spacings. A straight line would indicate homogenous extension (Chapman and Williams, 1984). The vein displacement-distance graphs (Figure 4(c) and(d)) have profiles which are concave-upwards, although Figure 4(c) closely resembles a linear curve.

In the shore-line exposure, only the heave of the fault can be seen, as a three-dimensional view was not always possible, and slip-vectors were often eroded. Similarly, contraction could have been underestimated due to the recognition difficulties of reactivated faults in the shore exposure. The smallest measurable veins were of the order of 0.5 mm, which could lead to undersampling.

Marrett and Allmendinger (1992) discuss the importance of the contribution of small faults to regional extension, and state that 25-60% of the total extension in the Viking Graben may be accounted for by small faults. Scholz and Cowie (1990) believe that small faults do

not contribute significantly to total extension calculations, as the largest faults produce the most strain. For the purposes of this study, 'small' faults have been identified as those with a heave of under 20 mm, which is determined from the power-law scaling relationship graphs below. The variation between the extension on a large scale, and that on a smaller scale is possibly due to the undersampling of small faults.

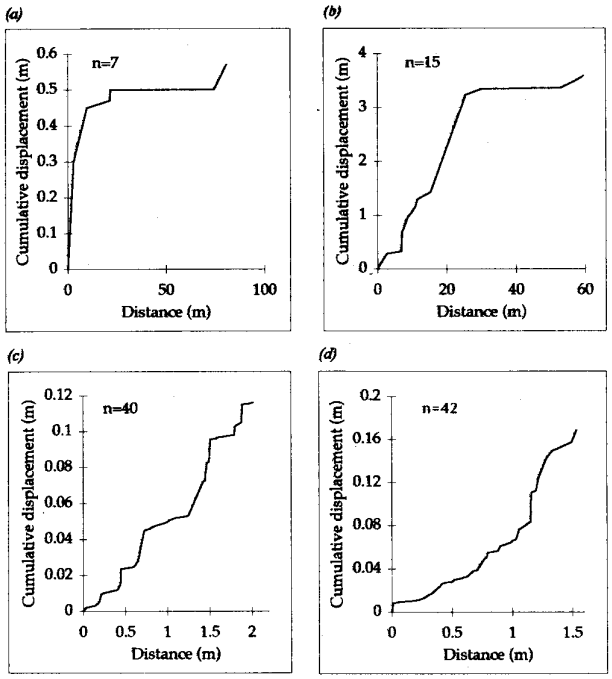

Figure 4. Cumulative displacement-distance graphs of north-south traverses for both faults and veins. (a) and (b) are examples of fault displacements, and (c) and (d) are examples of vein displacements.

Power-law scaling relationships.

Walsh and Watterson (1992) state that fault populations are related through a power-law distribution, that can then be used to quantify the number of faults of a given displacement:

$$N = C.\ U^{-D} \qquad \text{(Equation 2)}$$

Where N = the number of faults (veins) of displacement greater than U; D = the power-law exponent; and C= a constant. The faults and the veins at Kilve were each tested for such a relationship. A graph for the cumulative frequency of the normal fault heave data is shown in Figure 5 (a). There is a linear relationship covering almost three orders of magnitude for heaves in the range of 0.02 -10 m. There is a lower frequency with faults with displacements of between 0.2 and 1 m, which is possibly related to a resolution problem caused by sampling techniques of the faults in the cliffs and on the wave-cut platform. For the faults in the cliff the heaves were calculated trigonometrically from the dip of the fault plane, and the amount of throw, whilst the heaves of the faults exposed on the wave-cut platform were measured directly in the field. The gradient of the line is -0.47, and C is equal to 13.8. Other examples of power-laws for fault displacements are given by Peacock and Sanderson (1994), Marrett and Allmendinger (1992) and Scholz and Cowie (1990).

For the east-west striking veins, the cumulative frequency of the vein widths is plotted, and the results are shown in Figure 5 (b). There are two distinct linear relationships. The first is for vein widths of between 0.0005 and 0.009 m. The gradient of this line is -0.61, and C is equal to 0.09. The second linear power-law relationship is for veins with a displacement of between 0.009 and 0.04 metres for which the gradient is -1.21, and C is equal to 0.01.

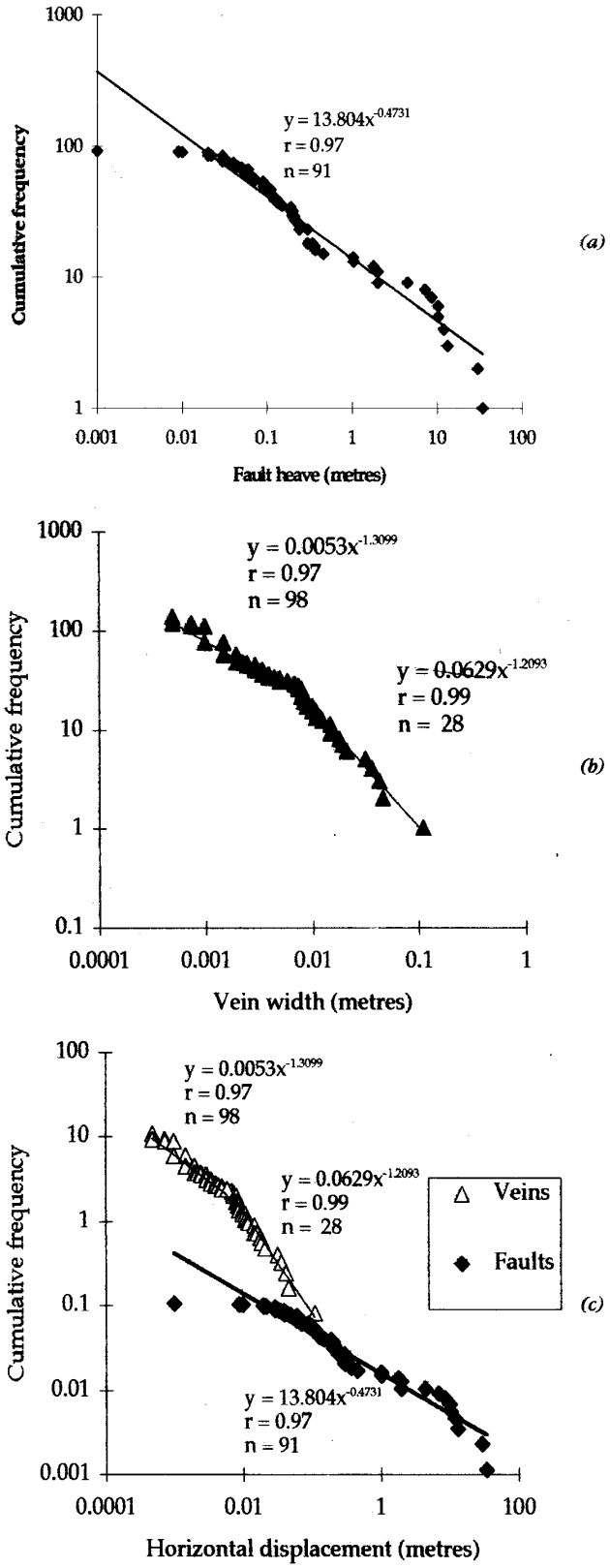

Figure 5. (a) Log-log graph of cumulative frequency of fault displacements. A linear relationship exists for displacements between 0.02 and 10 metres. (b) Log-log graph of the cumulative frequency of vein widths, showing two power-law relationships. One for displacements of 0.0005 and 0.009 m, and the second for displacements of 0.009 and 0.1 m. (c) A log-log graph combining vein widths and fault displacements against cumulative frequency per metre for comparison.

The gradient of the second line is too steep to fit in with the usual power-law distribution described by Walsh and Watterson (1992).

To analyse the scaling relationship of observed brittle structures at Kilve, the fault and vein power-law graphs were combined (Figure 5 (c)). The cumulative frequencies of the faults and veins were normalized to show the cumulative frequencies of the amount of fractures per metre. Along the length of a fracture trace, the displacement is transferred from a vein without vertical offset, at the fracture tip, to a small fault with both heave and throw. This leads to the occurrence of a hybrid fracture that is a combination of the two end-members of faults and veins.

The vein data were collected in small representative areas, but the fault data were collected over the whole length of the mapped section (3 km). Reactivation of normal faults may have caused the finite displacement to be less than the initial displacement frequencies. Fault and vein power-law relationships therefore warrant separate consideration, but the graph in Figure 5 (c) indicates similar scaling properties between vein populations with widths of less than 0.009 m and faults. The greater number of veins is a function of the sampling bias, i.e. veins were sampled in the wall-rocks where veining was more intense.

PALAEOSTRESS ANALYSIS

The quantification and determination of the palaeostress orientations is based on the fault-slip data collected for the strain analysis. This uses the FAULT-SLIP program that is based on Angelier's (1984) P-T dihedra method which calculates the most likely 'compression' and 'tension' orientations for a fault population.

For this method the fault plane, slip vector and the sense of movement are required. The fault plane data must also be divided into groups: reverse, normal or strike-slip faults. If any of these groups includes faulting from more than one event, then they should be further divided.

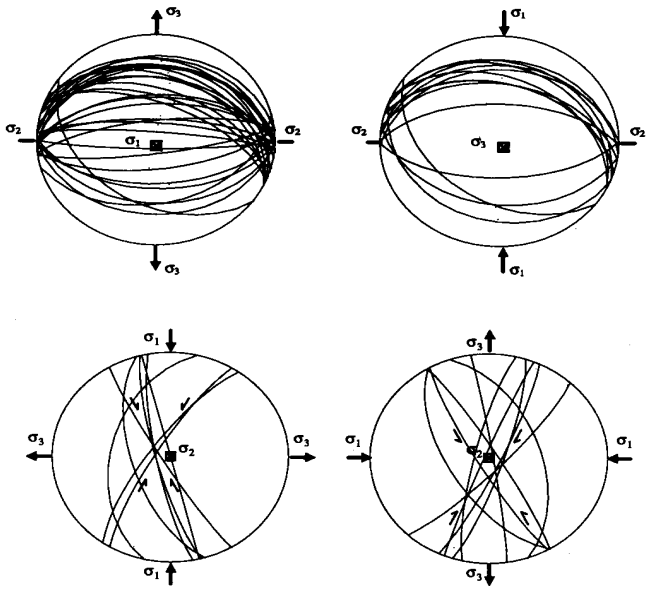

Figure 6. Equal area stereographic projections of the P-T Dihedra method, and the average orientations of the principal axes of stress. (a) normal faults, (b) reverse faults, (c) NE-SW dextral & NW-SE sinistral strike-slips, and (d) NW-SE dextral and NE-SW sinistral strike-slip faults.

Figure 6 shows the equal area stereographic projections of the fault planes and the most likely orientations of the stress axes. The maximum principal compressive stress axis is σ_1, σ_2 is the intermediate axis, and σ_3 is the minimum principal axis. The normal faults were caused by north-south extension, and the reverse faults were caused by north-south contraction. The strike- slip faults can be arranged into two distinct groups. The first shows north-south contraction, and the dextral faults have a strike of north-east—south-west, and the sinistral faults are orientated north-west—south-east. There are sinistral and dextral faults with the opposite movement senses (i.e. sinistral north-west—southeast, dextral north-east—south-west), that possibly infer east-west compression. However, there is an overlap in the data sets (Figure 3 (c) and (d)) suggesting that there is local variation in the stress axes orientations, inferring an apparent east-west contraction event.

Three different stress systems can be clearly identified, and a localized fourth system that needs clarification (work in progress), in which the three principal axes of stress are arranged in different orientations (Figure 6). Reverse faults and the north-east—southwest sinistral/north-west—south-east dextral faults are all indicative of north-south compression. If the P-T dihedra data for these two systems are added, a common a, (major principal axis of compressive stress) orientation can be resolved into a north-south orientation. The other two axes do not coincide, but may have inverted during the contraction, possibly due to similar magnitudes for σ_2 and σ_3. In strike-slip faults, the intermediate axis (σ_2) is vertical, and the principal axis of least stress is horizontal and oriented east-west. In reverse faulting the intermediate axis is horizontal, and east-west, and the minor axis (σ_3) is vertical. Sibson (1989) points out that stress systems can change during faulting episodes. Figure 7 shows the orientation of σ_1 common to both the reverse and the north-east—south-west sinistral/north-west—south-east dextral strike-slip faulting. Cross-cutting relationships observed in the field show that reverse and strike-slip faulting related to inversion post-dated normal faulting. The relative timing of the proposed east-west contraction is not clear, but the dihedral angle of these conjugate faults suggests that they are a feature of a later localised reactivation.

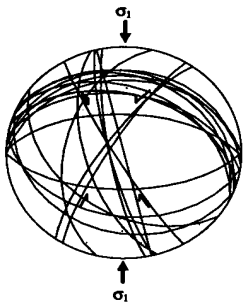

Figure 7. Equal area stereographic projection combining the reverse fault data with that of NW-SE dextral/NE-SW sinistral strike-slip faults.

Start Grid Reference	Length (metres)	Sum of heaves (metres)		%	%
		Extension	Contraction	Extension	Contraction
ST1488 4459	60	5.3	0	9.7	0
ST1483 4459	50	2.9	0.1	6.2	0.2
ST1477 4460	40	14.1	0.2	54.4	0.5
ST1474 4450	60	3.6	0.2	6.4	0.4
ST1460 4448	30	1.8	0.03	6.4	0.1
ST1452 4455	30	0.8	0.1	2.6	0.4
ST1442 4456	1.53	0.17	0	12.3	0
ST1428 4438	8.63	0.59	0	7.1	0
ST1423 4436	60	0.5	0.1	0.8	0.1
ST1394 4425	120	0.4	0.2	0.3	0.2
ST1373 4425	90	0.1	0	0.1	0
ST1355 4421	90	0.4	0.5	0.4	0.6
ST1331 4415	30	0.3	0	1.2	0
ST1310 4405	30	0	0	0	0
ST1290 4395	30	0.3	0	0.9	0
ST1270 4386	60	0.1	0	0.2	0
ST1238 4393	110	0.4	0	0.4	0

Table 1. Extension and contraction data for faults and veins.

CONCLUSIONS

i. Similar geometries are seen on mapping scales of 1:20 and 1:1250 for veins and normal faults.

ii. Minimum extension values are in the range of 7-12%, and minimum contraction is 0.2% using faults and veins.

iii. Individual power-law relationship exist for faults with displacements of between 0.02 and 10 m, vein widths in the range of 0.0005 and 0.009 m and a third power-law can be seen for veins with widths in the range of 0.009 and 0.1 m.

iv. North-south extension was followed by north-south contraction (which included reactivation) with associated strike-slip faulting.

ACKNOWLEDGEMENTS

We are grateful to M. Anderson and D.C.P. Peacock for their supervision, enthusiasm and advice. We would also like to thank D.J. Sanderson for the use of various strain and palaeostress programs, and a very helpful review. We are grateful for the help of Brian Williams and the anonymous reviewer.

REFERENCES

ANGELIER, J. 1984. Tectonic analysis of fault-slip data sets. *Journal of Geophysical Research,* **89,** 5835-5948.

CHAPMAN, T.J. AND WILLIAMS, G.D. 1984. Displacement-distance methods in the analysis of fold-thrust structures and linked faults systems. *Journal of the Geological Society of London,* **141,** 121-128.

MARRETT, R. AND ALLMENDINGER, R.W. 1990. Kinematic analysis of fault-slip data. *Journal of Structural Geology,* **12,** 973-986.

MARRETT, R. AND ALLMENDINGER, R.W. 1992. Amount of extension on "small" faults: an example from the Viking Graben. *Geology,* **20,** 47-50.

PEACOCK, D.C.P. 1991. A comparison between the displacement geometries of veins and normal faults at Kilve, Somerset. *Proceedings of the Ussher Society,* **7,** 363-367.

PEACOCK, D.C.P. AND SANDERSON, D.J. 1991. Displacements, segment linkage and relay ramps in normal fault zones. *Journal of Structural Geology,* **13,** 721-733.

PEACOCK, D.C.P. AND SANDERSON, D.J. 1994. Strain and scaling of faults in the Chalk at Flamborough Head, UK. *Journal of Structural Geology,* **16,** 97-107.

SCHOLZ, C.H. AND COWIE, P.A. 1990. Determination of total strain from faulting using slip measurements. *Nature,* **346,** 837-839.

SIBSON, R.H. 1989. Earthquake faulting as a structural process. *Journal of Structural Geology,* **11,** 1-14.

TURCOTTE, D.L., 1990. Implications of chaos, scale-invariance, and fractal statistics in geology. *Palaeogeography, Palaeoclimatology, Palaeoecology (Global and Planetary Change Section),* **89,** 301-308.

WALSH, J.J. AND WATTERSON, J. 1992. Populations of faults and fault displacement and their effects on estimates of fault-related regional extension. *Journal of Structural Geology,* **14,** 701-712.

WHITTAKER A. AND GREEN G.W., 1979. Weston-super-Mare Sheet 279 and parts of 263 and 295. 1:50 000 Series Solid and Drift Edition. *Geological Survey of Great Britain England and Wales.*

WILLIAMS, G.D. AND CHAPMAN, T.J. 1983. Strains developed in the hanging-walls of thrusts due to their slip/propagation rate: a dislocation model. *Journal of Structural Geology,* **5,** 563-571.